The structural characterization of amorphous thin films and coatings in their as-deposited state using x-rays at shallow angles of incidence

J. S. Rigden and R. J. Newport
Physics Laboratory, The University, Canterbury, Kent, CT2 7NR, United Kingdom

G. Bushnell-Wye
CLRC, Daresbury Laboratory, Daresbury, Warrington, WA4 4AD, United Kingdom

(Received 5 March 1996; accepted 1 October 1996)

We demonstrate the method of x-ray diffraction at shallow angles of incidence, using the intrinsically highly collimated x-ray beam generated by a synchrotron source, to study the atomic-scale structure of amorphous thin films and coatings in their as-deposited (i.e., on-substrate) state. As the incident angle is decreased, scattering from the film/coating can be isolated as contributions from the substrate are reduced. Systems studied include chemical vapor deposition (CVD) diamond films deposited onto both silicon and steel substrates, where evidence of an interfacial region between the film and silicon wafer has been observed, but we focus on a range of amorphous films/coatings (mixed $TiO_2 : SiO_2$ sol-gel spun films, hydrogenated carbon films and "glassy" carbon coatings, silicon: germanium semiconducting films and alumina coatings). The data are used both to comment upon the systems studied and to elucidate the potential, and the limitations, of the experimental method.

I. INTRODUCTION

The refractive index of materials at x-ray wavelengths is less than unity; consequently, at incident angles below a critical value, total external reflection occurs. Below this critical angle, α_c, limited penetration of the material is achieved via the evanescent mode, and is exponentially damped: in principle sampling depths of ~ 10 Å to ~ 1000 Å may be achieved. Above α_c, the penetration depth increases rapidly with incident angle, and inversely with the wavelength of the radiation, and is limited by photoelectric absorption. Thus, for a given wavelength, a number of characteristic sampling depths (length scales) may be achieved by varying the incident angle.

An experimental method for exploiting this phenomenon is the shallow angle diffraction technique, outlined originally by Lim and Ortiz[1] in their study of polycrystalline films (i.e., giving rise to sharp, Bragg diffraction peaks) deposited onto glass (i.e., amorphous substrates giving rise to weak, diffuse scattering only). Since their study required peak positions only, the method was well-conditioned for their problem. Even when relative peak amplitudes are useful, such as when Rietveld profile analysis of the crystallographic data is used, it is a relatively straightforward process to isolate the Bragg from any residual diffuse scattering, and the method has therefore been widely used in this form. However, a great many films and coatings of contemporary importance and interest are amorphous, and may be deposited onto (poly)crystalline substrates. Following a feasibility study by Burke *et al.*,[2,3] we have attempted to explore the potential of the generic method in this latter context in the hope of demonstrating that it is possible to isolate the structure factor and associated pair distribution function for an amorphous film—or at least to generate useful semiquantitative approximations. The method relies on the ability to use an intrinsically highly collimated, low divergence synchrotron radiation beam at shallow angles of incidence in order to limit the x-ray penetration depth, and thereby to render the substrate "invisible". It is the aim of this paper to demonstrate the potential, and the limitations, of the method within the context of a wide range of thin films and coatings.

II. THE MATERIALS

The last two decades have seen a growth in our knowledge of the properties of thin-film amorphous materials, accompanied by continued technological exploitation. The complex nature of these materials maintains their position of fundamental as well as technological interest, and important questions concerning their properties remain unanswered. In fact, the range of questions only increases as new and more novel materials continue to be generated.

 © 1997 Materials Research Society

A. Amorphous hydrogenated carbon (a–C:H) and CVD diamond films

Diamond has been used industrially for many years and has been exploited in capacitors, in the electronics industry, in bearings, and as high precision cutters. It has a unique combination of hardness and strength, a large dielectric constant, and an extremely low coefficient of friction. However, bulk diamond cannot be engineered into the many physical configurations required to exploit all these properties, and the recent advances allowing diamond to be grown as a thin film or coating have allowed the material to be used in a whole range of new areas, such as x-ray windows, electronic packaging applications, and friction and wear coatings.[4] Three diamond films of thickness ~ 5 μm were studied using shallow angle diffraction[5]: film A was a polycrystalline diamond thin film prepared by chemical vapor deposition (CVD) onto a polished silicon wafer; films B and C were both produced by microwave assisted CVD onto a steel disk: film B onto stainless steel, film C onto Invar steel. Two additional identical films were produced of film B and film C so that one film of each type could be removed from the substrate and examined by transmission diffraction to provide a useful benchmark for the shallow angle results. A description of the CVD process parameters is given in Refs. 6 and 7.

Amorphous hydrogenated carbon, a–C:H, is particularly interesting as it can be prepared harder, denser, and more resistant to chemical attack than any other solid hydrocarbon, and this leads to a broad range of potential technological applications. The macroscopic properties of a particular material are critically dependent on the conditions under which it was produced. a–C:H can be prepared in forms varying from the soft polymeric or graphitic at one extreme to a so-called "diamond-like" carbon form at the other. By altering the deposition parameters it is possible to vary, for example, properties such as the optical band gap and refractive index.[4b,8] The a–C:H sample discussed here was prepared using a saddle-field fast-atom (i.e., neutral particle) source with propane as the precursor gas; the deposition conditions pertain to the hard form of the sample (an effective beam energy of 1.3 kV, and operating at 1.4×10^{-4} mbar system pressure). The macroscopic sample density was determined as $1.7\ \mathrm{gm \cdot cm^{-3}}$ using a residual volume technique, and the hydrogen content was determined as 32 at.% using a Carlo-Erba CHN combustion analyzer. We have undertaken detailed neutron and x-ray scattering studies of the material in its powder (i.e., off-substrate) form and have been able to offer a new model for the atomic-scale structural properties of the material.[9] However, it is of interest to be able to study the structure of the film while still on a substrate, and ultimately to be able to comment on the effects of different substrates, heat treatment, etc.

B. a–Si:C:H and a–Si:Ge:H films

Codeposition with silicon to generate a–Si:C:H films offers the potential of variable bandgap semiconductors, and is of further interest in its photo-oxidized form within lithography,[10] but very little structural work has been done on these materials beyond spectroscopy[11] for the simple reason that large-volume, off-substrate samples are difficult to produce. This system is therefore a candidate for study using the shallow angle method. In a similar vein, a–Si:Ge:H, although overshadowed hitherto by the research on its analogue, amorphous hydrogenated silicon, a–Si:H, has enormous potential as a narrow-gap component of multijunction solar cells and other devices using amorphous semiconductors (Ref. 12 and references therein). Again, little direct (diffraction) work had been undertaken, although IR and TEM studies indicated a local structure similar to that of a–Si:H.[12] The a–Si:Ge:H was deposited by a conventional glow discharge method,[10] while the a–Si:Ge:H was produced by reactive magnetron cosputtering (two thin films of ~ 1 μm thickness were deposited at low rf power, 30 W, onto silicon wafers: a:Ge:H using a substrate temperature of 200 °C and a–Si:Ge:H with substrate temperature 225 °C[12]).

C. $SiO_2:TiO_2$ spun sol-gel films

Mixed silica: metal-oxide materials are of significant technological importance. Silica glasses with a few mol% TiO_2 are used as ultralow thermal expansion (ULE) glasses,[13] and mixed titanium: silicon oxides are important as catalysts and catalytic support materials.[14] In the optical industry they are produced as antireflective thin film coatings, with tailored refractive indices. The properties of titania: silica binaries, however, are strongly dependent on their chemical composition, homogeneity, and texture. Sol-gel synthesis, based on hydrolysis of metal alkoxide precursors, and subsequent condensation, is a relatively new method that combines atomic level mixing with a high degree of porosity. Ti and Si alkoxides have very different hydrolysis rates that can mean phase separation occurs as Ti-rich and Si-rich regions form. ^{17}O NMR has confirmed that atomic mixing occurs in such glasses by revealing the presence of Ti–O–Si bonds[15,16]; in contrast, OTi_3 and OTi_4 features in the NMR spectra[17] of glasses with higher TiO_2 content (~ 41 mol%) indicate that they are phase separated.

Although much work exists on the sol-gel process, details of the atomic-scale structure remain elusive; this problem may usefully be addressed using advanced spectroscopic and scattering techniques. Silica and silica: titania binaries have been studied in their crystalline phases using x-ray diffraction,[18,19] but relatively little work has been undertaken on the gels in their amorphous

state.[20] Transmission x-ray or neutron diffraction can reveal structural information averaged over an entire sample, and is therefore a useful method for studying bulk material. However, conventional techniques cannot be used to study thin films or coatings, due to the difficulty in separating the signal arising from the film from that of the substrate. Shallow angle x-ray diffraction can enable structural information from a thin film to be isolated.

The SiO_2-TiO_2 mixed gels were prepared by hydrolysis of titanium *n*-propoxide ($Ti(OPr^n)_4$) and tetraethoxy orthosilicate (TEOS). The sol-gel glasses were prepared with water and propanol mixtures in the approximate ratios 1:2:7.5, with varying titania contents. Sample 1, labeled 'pure silica', contained no titania, samples 2 and 3 contained small, differing amounts of titania and were labeled 'low titania' and 'high titania', respectively. Full details of the sample preparation and characterization are given elsewhere.[16,20,21] Table I shows the compositional information, including mass and electron densities. The precursor sols were used to produce thin films by the spin coating method.[13] An excess of liquid is dropped onto the surface of the substrate, and then the sample is rotated at low speed so that the liquid flows radially outward, driven by centripetal force. Surplus liquid flows to the edge of the substrate and drips off. As the film thins, the rate of removal of liquid slows down as the viscosity increases; in the final stages most of the thinning occurs by evaporation of volatiles.[22] This method produces a very uniformly thin coating, and the process may be repeated several times to build up a thicker film or, for example, to produce layers with slightly differing qualities. In the present case, six layers of film were deposited from the same stock mixture to produce a film ~ 1 μm thick on a polished silicon wafer.

Although the underlying physics and chemistry that govern growth and gelation are the same for films and bulk sol-gels, several factors in the evolution of thin films mean that, structurally, the two forms may be quite different.[13] In bulk systems evaporation usually occurs after gelation, whereas in thin films the deposition and evaporation processes occur simultaneously, and this results in a competition between compaction of the structure caused by evaporation and the stiffening (and therefore resistance to compaction) of the material caused by the structural condensation process. The short duration of deposition and evaporation/drying in thin films means that considerably less crosslinking occurs than in bulk gels, which generally results in more compact dried structures; this is particularly true for films made by spinning methods. Also, thin films are constrained by their geometry, and the continued shrinking causes stresses. It is likely, therefore, that the rapid gelation of thin films will result in a more disordered material than in the bulk with a lower concentration of volatiles.

D. Alumina and "glassy" carbon coatings

Graphite is used as an electrode material in a great many applications from fuel cell technologies to the potentially aggressive environments associated with vacuum furnaces, plasma deposition/etching systems, and so on. Being porous, the material can be problematic in the context of out-gassing and contaminant ingress; its structure also leads to problems of particulate generation within the system. These problems can be significantly alleviated, and the uniformity of the surface electrical and thermal conductivity improved, without an associated degradation in the levels of chemical purity, if the graphite surface is suitably treated. We have used a sample of a commercially produced "glassy" carbon coating (~ 5 μm thick) in which the graphite is impregnated with a carbon-based solution and then heat-treated to temperatures of 1800 °C in a high vacuum in order to explore the potential of the method for isolating near-surface changes, even for low atomic number materials.

In a similar vein, protective/functional coatings of hard, inert materials such as alumina are of interest. However, these are often required to be very thin and to be in a particular chemical/physical state since it is the attributes of the substrate that are paramount to the application and these must not be compromised by the coating material itself. We have used two electron beam

TABLE I. Compositional information for the four samples studied; the figures in parentheses in column 1 refer to the mol % of TiO_2.

Sample		Composition, at. %					Density	Electrons
		Ti	Si	O	C	H	$g \cdot cm^{-3}$ (atoms $Å^{-3}$)	per $Å^3$
1	Pure SiO_2	0.0	4.0	16.2	21.6	58.6	2.25 (0.20)	0.736
2	Low titania, $SiO_2:TiO_2$ (8%)	0.4	4.7	19.7	20.2	55.5	2.45 (0.19)	0.789
3	High titania, $SiO_2:TiO_2$ (18%)	0.84	3.8	17.0	21.0	57.3	2.65 (0.22)	0.856
4	Phase separated, $SiO_2:TiO_2$ (41%)	4.9	7.0	38.2	7.0	42.7	3.10 (0.16)	0.954

deposited samples of thin (0.5 μm thick) Al_2O_3 films on silicon single crystal substrates produced in an industrial research laboratory. One of the samples was deposited in the presence of a 500 kV ion beam (labeled #91), which on the basis of existing experimental evidence would be expected not only to result in a denser film, but possibly also to alter the degree of crystallinity associated with conventionally deposited films. The shallow-angle-of-incidence method provides a diffraction pattern which is a weighted average of the entire probed volume, and given the large illuminated area (in this case ~ 5 cm^2) the data will be well-conditioned to reveal the presence of Bragg-like (crystalline) peaks in an otherwise diffuse (amorphous) spectrum that might not be revealed by more conventional selected-area probes.

III. THE SHALLOW ANGLE TECHNIQUE

When electromagnetic radiation is incident at an angle α_i, upon a material with a critical angle for external reflection α_c, it will be affected in one of four ways: (i) if $\alpha_i < \alpha_c$, the radiation is totally externally reflected; (ii) if $\alpha_i = \alpha_c$ the refracted beam propagates parallel to the surface of the sample; (iii) if $\alpha_i > \alpha_c$, the refracted beam passes into the sample, and the near-surface region will be illuminated to a characteristic penetration depth t, as in Fig. 1; (iv) if $\alpha_i \gg \alpha_c$ the refracted beam penetrates through the sample into the interface layer or substrate.

For a material of density ρ g cm^{-3}, and an incident wavelength λ in Å, α_c (in radians) is given by:

$$\alpha_c = 1.6 \times 10^{-3}\, \rho \frac{1}{2} \lambda \tag{1}$$

For an incident angle $\alpha_i < \alpha_c$, the near surface region of the material will be illuminated to a depth t at which the electric field vector has fallen to $1/e$, where t is given by:

$$t_{\alpha_i} < \alpha_c = \frac{\lambda}{2\pi(\alpha_c^2 - \alpha_i^2)^{\frac{1}{2}}} . \tag{2}$$

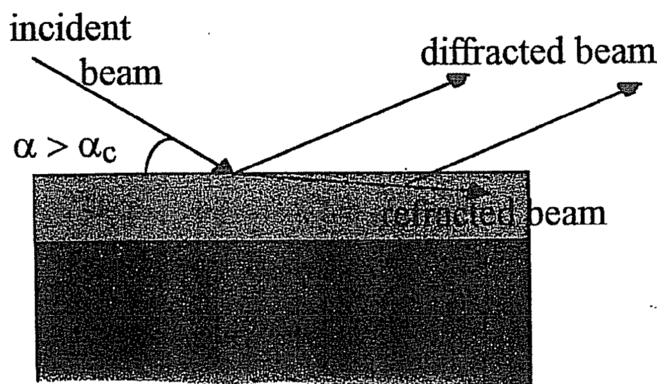

FIG. 1. Geometry for diffraction to occur at shallow angles of incidence.

Above α_c, penetration into the material increases rapidly with the incident angle. If α_i is larger than α_c but still small we have[23].

$$t_{\alpha_i > \alpha_c} = \frac{2\alpha_i}{\mu} \tag{3}$$

where μ is the (wavelength dependent) linear attenuation coefficient given by the product of the mass attenuation coefficient and the density.

For example, for a diamond thin film, typically of density 3.52 g cm^{-3}, at an incident x-ray wavelength of 0.5 Å, α_c = 1.5 mrad = 0.086° and μ_c = 1.18 cm^{-1}. For a silicon wafer, however, μ_{Si} = 5.57 cm^{-1}; since both the mass attenuation coefficient and density for all steels are high, μ_{steel} is also large; penetration of x-rays into steel at shallow angles is therefore negligible. Table II shows the contrast in penetration depths t for a variety of incident angles α_i, just above α_c, for this example of diamond film and substrates. An incident angle of 0.05° is just below α_c for diamond at an x-ray wavelength of 0.5 Å, and hence Eq. (2) would be used to calculate the penetration depth; t is therefore 1.2 μm in this case.

IV. EXPERIMENTAL METHOD

The conventional $\theta:2\theta$ transmission and shallow angle x-ray diffraction data presented here were collected on Station 9.1 at the Synchrotron Radiation Source (SRS) at the Daresbury Laboratory, U.K.[24] The intrinsically highly parallel nature of the beam provided by a synchrotron radiation source is of advantage over conventional focused laboratory x-ray sources for the shallow angle technique in that the associated serious geometric aberration effects are avoided. Further, the high intensity beam provided by a synchrotron source is necessary for the relatively weak, diffuse scattering from the small volume of material sampled in the shallow angle geometry; the availability of relatively hard x-rays allows a wide dynamic range (up to ~ 18 Å^{-1}).

The conventional (transmission) x-ray diffraction arrangement is modified to produce the shallow angle configuration; this instrument configuration is shown

TABLE II. Penetration depth for x-rays incident at an angle $\alpha_i > \alpha_c$ onto diamond, silicon, and steel.

Incident angle	Penetration depth, t μm at λ = 0.5 Å		
α_i°	Diamond film	Silicon wafer	Steel disk
2.0	590	125	0
1.0	295	62	0
0.5	148	31	0
0.2	59	12	0
0.1	30	6	0

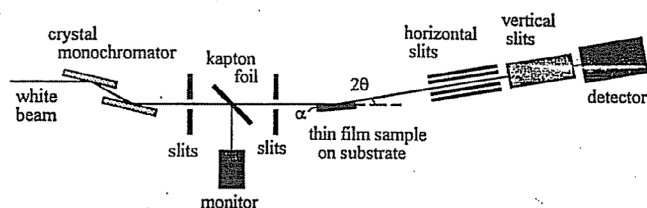

FIG. 2. The instrumental arrangement for diffraction at shallow angles of incidence.

schematically in Fig. 2. In both cases, the white beam from the synchrotron source is monochromated by a channel cut crystal and proceeds through a pair of slits which define the incident beam profile. A slit of ~0.8 mm by 10 mm is used for transmission work to maximize the scattered beam intensity. A narrow slit profile of 100 μm by 10 mm is used in shallow angle work to limit contamination from the straight through beam at the lowest incident angles. For transmission diffraction, the angle θ of the sample, normal to the incident beam, is coupled to the position of the detector 2θ; this facilitates sample corrections by producing a simple, $\cos(\theta)$ dependence in the volume of illuminated sample. The scattered radiation passes through a simple slit system to the detector where data are collected sequentially at angles $2\theta = 2°$ to $130°$.

For shallow angle diffraction, the sample is set at a fixed, small angle α_i to the incident x-rays. An iterative procedure of height and angle adjustment is used to define the zero-angle for the sample[2,3]; this procedure is very important given the small angles used in data collection. It is also essential that the sample is smooth and flat; any significant irregularity in the film thickness will produce an uncertainty in α_i and hence on the collected scattering profile. The scattered radiation passes through an arrangement of horizontal and vertical slits to the detector. A long slit package reduces the angular spread of scattered radiation incident on the detector and results in a resolution of ~0.07°. Data are collected in the same angular range as in the standard transmission case, later converted to scattering vector $|\mathbf{Q}| = (4\pi/\lambda)\sin\theta$.

V. DATA ANALYSIS

There are many texts detailing x-ray diffraction theory, for example Ref. 25, and this will not be presented here. Basic data reduction for both conventional and shallow angle x-ray diffraction can be carried out in a similar manner; i.e., corrections are made for detector dead time, changes in incident beam current, and beam polarization effects.[25] A further correction is needed in the shallow angle geometry to account for the fact that the x-ray beam collected at the detector is actually scattered from the *refracted* beam in the sample; this produces a small shift in the measured scattering angle 2θ.[3]

More sample-specific corrections, such as sample absorption and multiple scattering and conversion to absolute units, are not included in the reduction procedure for the shallow angle technique. Both are complicated by unknown factors in the sample geometry, which means it is difficult to measure the actual penetration depth into the sample and/or substrate and therefore the contribution to absorption effects from each. This situation could be clarified if the films were thick enough to ensure that the incident x-rays did not penetrate to the substrate. This would, however, limit the usefulness of the technique as a probe sensitive to different depths of the thin film, such as surface or interlayer effects. Reduction of the incident angle or increasing the incident x-ray wavelength reduces the need for very thick samples and alleviates this problem somewhat; however, increasing λ decreases the Q range and therefore the real-space resolution following Fourier transformation. Subtraction of the background scattering in the shallow angle geometry can also be problematic, as it is in essence impossible to measure. However, for scattering from crystalline materials, where the bulk of the scattering is concentrated in sharp Bragg reflections, this does not reduce the amount of information obtainable from the data.

VI. RESULTS AND DISCUSSION

A. a–C:H, a–Si:C:H, and CVD diamond films

Diffraction data for the CVD diamond film deposited onto a silicon wafer were collected at an incident x-ray wavelength of 0.5 Å and at sample angles α_i of 2.0°, 1.0°, 0.5°, 0.2°, and 0.1°.[5] Figure 3 shows a comparison of the corrected shallow angle scattering profiles, with highest α_i uppermost; Table III gives the positions of the major peaks in each data set. It is immediately clear that the sharp peaks associated with the silicon substrate, such as those at ~9.7 Å^{-1} and ~11.5 Å^{-1}, decrease rapidly when the incident angle is decreased (and therefore the penetration depth into the sample/substrate falls), whereas those associated with the diamond film, e.g., the diamond {111}, {220}, and {311} reflections at 3.05, 4.98, and 5.83 Å^{-1}, increase as α_i approaches α_c. The silicon peaks at higher Q become less sharp and other diamond peaks such as those at ~9 Å^{-1} {511} appear as scattering from the thin film is isolated.

The two peaks at ~17.1 and ~19.4 Å^{-1} do not follow this trend. In fact, the peaks sharpen at a penetration depth corresponding to $\alpha_i = 1.0°$ and shift to slightly shorter Q-values (larger d spacing). This may indicate that the penetration depths associated with this geometry probe a highly ordered Si–C interfacial layer between

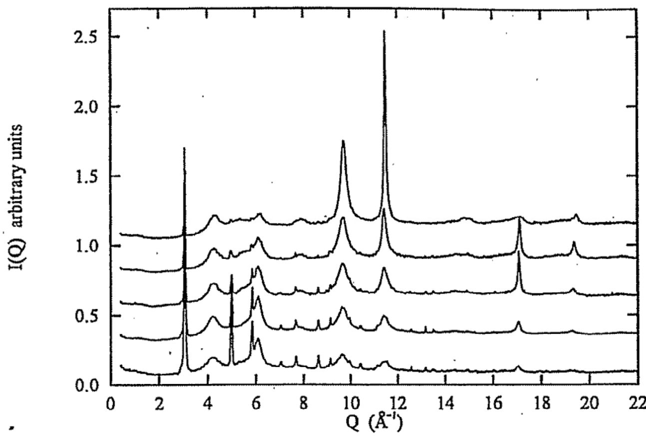

FIG. 3. Scattering from the CVD diamond thin film sample 'A' deposited on silicon at a variety of incident angles; from top to bottom α_i = 2.0°, 1.0°, 0.5°, 0.2°, and 0.1°.

the silicon and diamond. (Silicon : carbon interfacial regions have been observed by many workers using other probes/methods; see, for example, Refs. 7 and 26 and references therein.) The peak at ~6.1 Å^{-1}, tentatively assigned to silicon, also exhibits some unusual characteristics: it is broad at higher values of α_i, but appears to become sharper as the incident angle is decreased, suggesting it is a feature associated with the film, not the substrate. However, its presence in the α_i = 2.0° scan, which has little contribution from the diamond film, indicates the contrary: it may be that the peak appears more intense due to the sharpening of the diamond peak at 5.83 Å^{-1} on its low-Q side. Alternatively, this peak could be near-surface graphitic material which would exhibit diffracted intensity in the same region (however, lower order graphitic reflections are not visible, which casts some doubt on this speculation).

The CVD diamond films on steel disks were examined using an x-ray wavelength of 0.7 Å, slightly higher than for film A. A higher incident wavelength means that the penetration depth for each α_i is decreased, but the available Q-range measurable is reduced. For materials exhibiting Bragg scattering this is convenient as structural information is concentrated at lower Q-values, with the advantage that the need for thicker films is lessened. Data were collected at incident angles of 0.05°, 0.1°, and 2.0°; however, it was found that at all incident angles a contribution from the substrate was visible to some extent. There are several possible reasons for this: the film could be thinner than estimated so that incident x-rays always penetrate through to the substrate below; there could be cracks or irregularities in the film such that the steel is effectively more visible; or the surface of the steel could be very rough so that the interface layer is wide and hence effectively near the surface. Since the surface of the steel disk was

TABLE III. Major peak positions in the shallow angle data of CVD diamond deposited on silicon for various α_i, with peak assignments: D: diamond, Si: silicon, Si–C: silicon-carbon.

α_i°	Major peak positions in Q ± 0.02 (Å^{-1})								
2.0	3.05	4.32			6.15		7.84		8.60
1.0	3.05	4.23	4.98	5.83	6.11		7.66		
0.5	3.05	4.23	4.98		6.10	6.95	7.66		8.64
0.2	3.02	4.23	4.98	5.83	6.06	7.05	7.66		8.64
0.1	3.05	4.23	4.98	5.83	6.06	7.00	7.67	8.04	8.64
Assignment	D	Si	D	D	Si	D	D	D	D

α_i°	Major peak positions in Q ± 0.02 (Å^{-1})								
2.0		9.72				11.56	14.92	17.11	19.45
1.0	9.12	9.72				11.46	14.94	17.10	19.40
0.5	9.16	9.63		10.43		11.42	14.52	17.10	19.35
0.2	9.16	9.67	9.96	10.43		11.42		17.05	
0.1	9.16	9.63	9.96	10.43	11.13	11.46		17.00	
Assignment	DD	SiD	DD	DD	DD	SiD	SiD	Si/Si–CD	Si/Si–CD

prepared by shock implantation[6,7] to enhance nucleation, the surface will be rough; the latter option is therefore considered the most likely. Further work is underway to study CVD diamond on polished steel.

Figure 4 shows scattering from films B and C at a shallow angle of 0.05° and incident x-ray wavelength of 0.7 Å, compared with transmission diffraction measurements of identical films removed from the substrate. Transmission diffraction will give information on the averaged structure throughout the film; i.e., it is not possible to distinguish the structure in the bulk of the film and in the interface or surface regions. The transmission measurements are therefore expected to contain information predominantly on the bulk of the sample, whereas shallow angle measurements will be sensitive to structural information at a penetration depth determined by the angle of incidence. This could be associated with the film, interface region, or substrate, or most likely as a weighted mean of these components.

The scattering from film B, off substrate, reveals clear Bragg peaks at positions and reflections corresponding to a diamond arrangement: 3.06 {111}, 4.98 {220}, 5.86 {311}, 7.04 {400}, 7.70 {331}, 8.62 {422}, 9.19 {511}, 9.97 {440}, and 10.41 $Å^{-1}$ {531}; there are no other strong Bragg peaks. Similarly, for film C, off substrate, the significant peaks result from diamond reflections, although an additional peak is clear at 3.49 $Å^{-1}$, thought to result from a graphite {102} reflection. This suggests that there is indeed a small amount of graphitic carbon within the sample. The shallow angle results for film B, however, show many strong non-diamond peaks, indicating that even at $\alpha_i = 0.05°$ the x-rays have penetrated to the steel substrate. Table IV shows the major peak positions in the region $Q = 2.5$ to 4.5 $Å^{-1}$, together with tentative assignments where possible. Strong Bragg peaks from graphite, iron, and nickel are visible, as are several more sharp peaks originating from other, less easily defined, constituents of the steel disk—or just as likely, one or more metal carbides (e.g., manganese carbide). In particular, two additional strong peaks are present on either side of the diamond {111} peak at 3.06 $Å^{-1}$, the graphite {100} peak at 2.98 $Å^{-1}$, and the iron {110} peak at 3.10 $Å^{-1}$. In contrast, the shallow angle diffraction pattern from film C shows very little contamination from the steel substrate, and the visible Bragg peaks result from the expected diamond structure but also graphite interlayer distances. The latter peaks are probably due to graphitic structure in the film, perhaps in the interface or surface region. It is important to note, however, that these results are not consistent with there being a significant proportion of metal carbides present in the film.

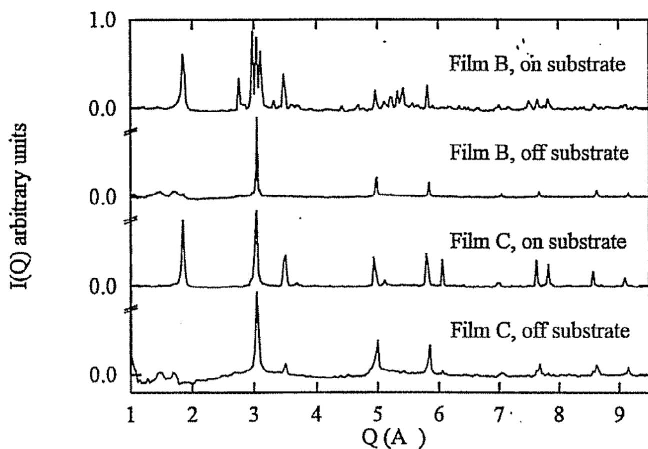

FIG. 4. Scattering from the CVD diamond on steel (samples 'B' and 'C') showing a comparison of the two films and the transmission and shallow angle diffraction results.

While the thin film structure has not been completely isolated at $\alpha_i = 0.1°$, the reduction in scattering from the substrates (particularly silicon) is significant; the sample scattering could be isolated further by reducing the angle of incidence to lower angles (and improving the collimation package of the detector). The data presented here were collected at x-ray wavelengths of 0.5 Å. Increasing this would increase the attenuation coefficient for the film, thereby reducing the penetration depth and achieving the same effect, albeit at the expense of a reduction in Q-range. For crystalline samples this would be the favorable option as structural identification can be achieved from a more limited range of reciprocal space data. The comparison of the CVD diamond films deposited onto steel disks examined in their as-deposited state by shallow angle diffraction, and off-substrate by conventional transmission x-ray diffraction, revealed that the shallow angle data showed contributions from the scattering from the steel. This may be due, in part, to the steel being initially prepared by the shock implantation of diamond as a base for the CVD process.

TABLE IV. Prominent peak positions in the shallow angle data of films B and C in the range 2.50 to 4.50 $Å^{-1}$, with peak assignments: D: diamond, G: graphite, Fe: iron, Ni: nickel, and ?: unknown.

Film	Mode	Peaks in Q-range 2.50 to 4.50 $Å^{-1}$ in $Q \pm 0.02$ ($Å^{-1}$)									
B	Shallow	2.76	2.85	2.98	3.05	3.10	3.32	3.49	3.61	3.70	4.41
C	Shallow				3.06			3.50		3.70	
Assignment		?	?	G	D	Fe	?	G	Ni	G	Fe

Our data relating to a–C:H and a–Si:C:H, which were found to be very similar in the context of this project, have been published in detail elsewhere.[9,10] A comparison between the pair distribution function derived from conventional $\theta : 2\theta$ transmission data from a "powder" sample and that from the as-deposited analogue derived from shallow angle experiments is shown in Fig. 5 for the a–C:H case. The conclusions of that program may be summarized briefly as a confirmation that there is no significant difference between the atomic scale structure of the thin-film (as-deposited) material and its thicker, off-substrate powder analogue. These experiments did, however, reveal a limitation to the shallow angle method in that the difficulty of isolating amorphous film from crystalline substrate becomes very difficult when using materials of low atomic number.

B. a–Si:Ge:H films

Data for the a–Si:Ge:H systems are presented here for the first time. The scattering from each sample, orientated at angles α_i of 5.0°, 2.0°, 0.5°, 0.1°, and 0.05° to the incident beam, was collected in a scattering angle range of 2θ = 2° to 130°, corresponding to a Q-range of 0.25 to 16.5 Å^{-1} for an x-ray wavelength λ = 0.69 Å. Figures 6 and 7 show the interference functions (i.e., our approximation to the structure factor) obtained by subtracting the Chebyshev polynomial from each set of data for the two samples, as detailed above. The interference functions vary in a similar way, and the evolution of the interference function for a–Si:Ge:H is described in detail below.

1. At the shallow angle α_i = 2.0°, sharp peaks can be observed in the interference function corresponding to Bragg peaks from the crystalline silicon substrate. In particular, the Si{333} reflection at 6.02 Å^{-1} is very strong and is not present in any of the other data sets. Wider peaks are also observed at Q = 1.97 and 3.48 Å^{-1}; the first of these most probably corresponds to the Si{111} reflection. However, it is not as clear what the other feature is associated with. It could be due to a combination of the Si{220} and {311} reflections alone, but might conceivably include a contribution from a {310} reflection arising from a site-disordered Si–Ge lattice in the interfacial region. Likewise, the peak we have assigned as Si{111} may have a contribution from the reduced-symmetry interface which contributes to its observed width. The data are somewhat ambiguous, although we are clearly probing the silicon wafer in this scan, which is dominating the scattered intensity.

2. At α_i = 0.5°, the sharp Bragg peaks from the silicon wafer at higher values of 2θ have significantly decreased. However, the first two peaks have increased in intensity and moved slightly (to 1.94 Å^{-1} and 3.51 Å^{-1}). Both these positions are more in line with the {111} and {310} reflections of a Si–Ge lattice, if we assume that the Si and Ge sites within the Si (diamond) lattice

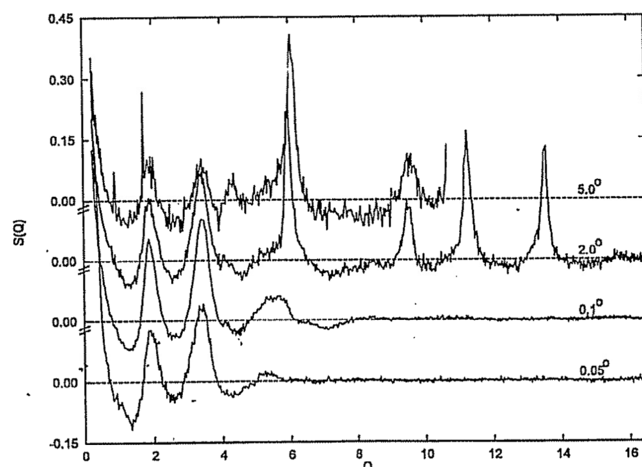

FIG. 6. The measured interference function for the a–Ge:H film using the shallow angle method.

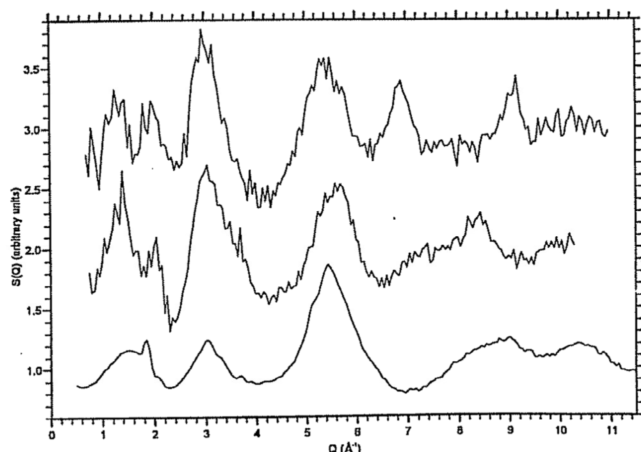

FIG. 5. A comparison of $\theta : 2\theta$ (transmission) and shallow angle interference functions (approximate structure factors) for a–C:H.

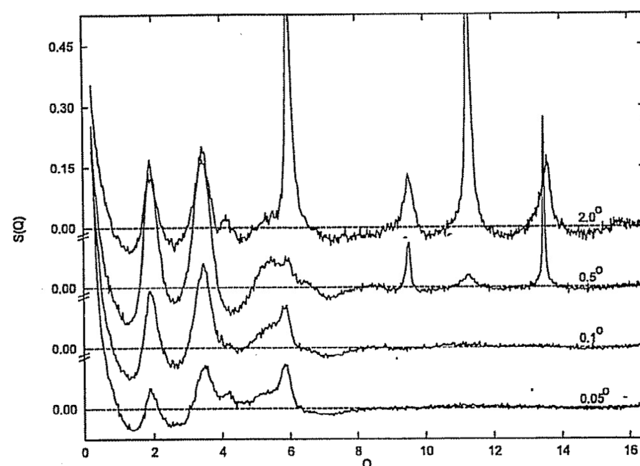

FIG. 7. The measured interference function for the a–Si:Ge:H film using the shallow angle method.

are interchangeable by random substitution, with just bond lengths varying according to the pairs of atoms involved. A sharp peak at 13.48 $Å^{-1}$ also appears in this scan but not in the others; this may be a Si or Si–Ge Bragg peak. All the features are very sharp, and it is now highly likely that they include scattering from a (crystalline) interfacial layer between the Si wafer and the a–Si : Ge : H film.

3. At $\alpha_i = 0.1°$, the structure is evidently more amorphous with no sharp Bragg peaks present, but the peak profile is significantly sharper than that expected from a truly amorphous structure. Peak positions can still be associated with a Si–Ge diamond-like lattice.

4. By $\alpha_i = 0.05°$ the first two main scattering peaks are much less pronounced and have moved to positions associated with a Si–Ge structure. Indeed, there is much similarity between these data and those available for bulk samples of a–Si : H.[27] The peaks are much wider and less pronounced than at higher angles of incidence, which suggests that we have probed to a much shallower depth and contributions from the crystalline substrate have indeed been successfully eliminated.

The interference functions for the a–Ge : H sample are very similar, but there is no peak at ~ 6 $Å^{-1}$; this feature results from Si : Si distances. The comparison of the interference functions for the 0.05° shallow angle scan for both samples is shown in Fig. 8. It is clear that, at very shallow angles of incidence, the scattering from these amorphous films can indeed be isolated. These results suggest, as might be anticipated, that the thin film of a–Si : Ge : H exhibits an atomic structure very similar to an amorphous analogue of a diamond-like lattice, with Si and Ge atoms interchangeable at the sites on a random substitutional basis. The presence of a more strongly crystalline interfacial layer is also suggested, where the crystallinity of the Si wafer imposes some ordering onto the conformation of the deposited alloy. Further evidence for this conjecture is of course provided by the Fourier transform of the interference function, which reveals pair correlations at those distances one might expect on the basis of the additive use of published covalent radii, and bond angles very close to the anticipated tetrahedral value (Fig. 9).

C. $SiO_2 : TiO_2$ spun sol-gel films

Figure 10 shows the corrected data for the three sol-gel samples after fitting and subtracting a polynomial from the data. The scattering from the samples containing titania looks very similar, but the 'pure silica' sample shows a much stronger scattering across the whole Q-range. Small Bragg peaks due to the silicon substrate are visible at 6.0 and 9.5 $Å^{-1}$ (the {511} and {800}, respectively) and at 13.5 $Å^{-1}$ in the 'pure silica' and 'low titania' samples, although only the peak at ~ 6 $Å^{-1}$ appears

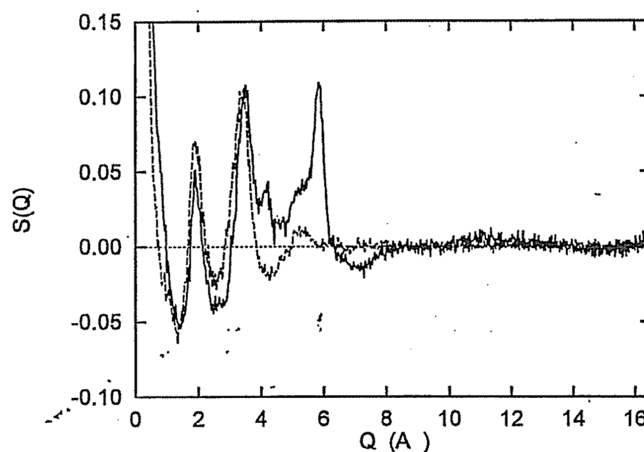

FIG. 8. A comparison of the interference functions for a–Ge : H and a–Si : Ge : H at $\alpha_i = 0.05°$.

to be present in the 'high titania' sample. This is likely to be due to the fact that the higher titania film is more electron-dense and therefore the incident beam is attenuated more strongly. This observation, coupled with the fact that the silicon peaks are very small, suggests that the penetration depth covered by the incident x-rays is only just greater than the thickness of the films, and so penetration into the silicon wafer is small. The sharpness of the first sol-gel peak in the 'pure silica' data at ~ 1.9 $Å^{-1}$ may, in addition, indicate contamination from an underlying residual silicon Bragg reflection.

The interference functions reveal the similarities between the scattering from all three samples after the first major peak. It is clear that the visible Bragg peaks, particularly the one at ~ 6 $Å^{-1}$, represent a significant problem if analysis were to continue by way of conventional direct Fourier transform to a pair distribution function, $G(r)$; their presence could lead to strong silicon correlations in the $G(r)$. However, the rapid decay of the data to the asymptotic value,

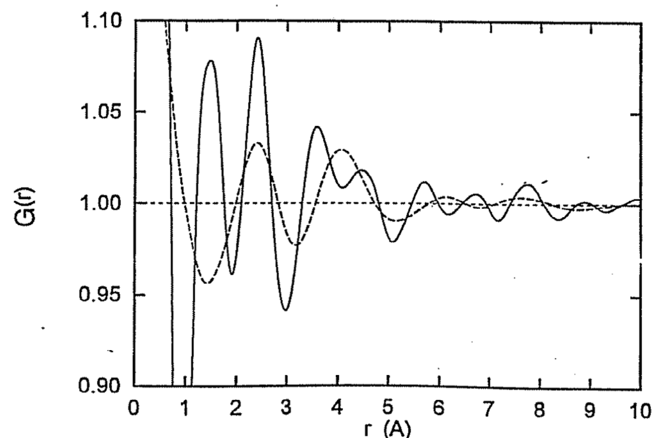

FIG. 9. A comparison of the (approximate) pair distribution functions for a–Ge : H and a–Si : Ge : H at $\alpha_i = 0.05°$.

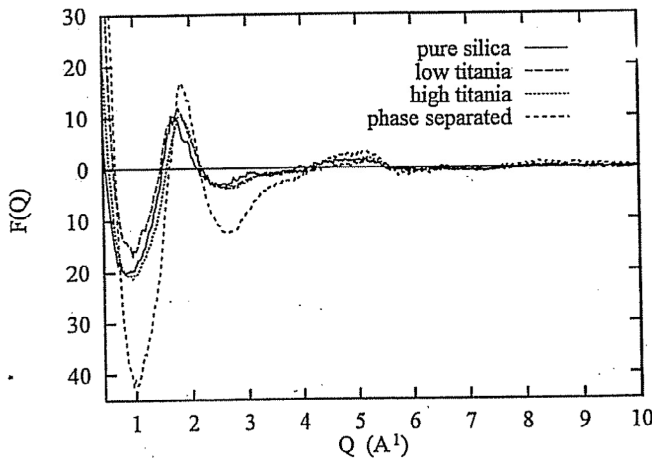

FIG. 10. Corrected interference functions for the three sol-gel films.

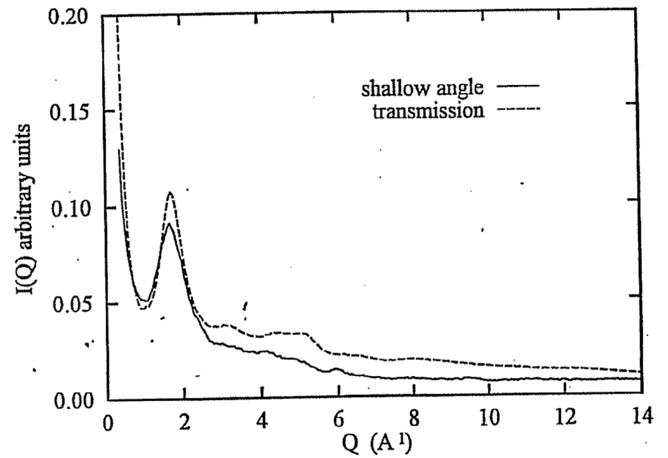

FIG. 11. A comparison of $\theta:2\theta$ (transmission) and shallow angle interference functions for the "high titania" mixed sol-gel glass.

after the first sharp peak at ~ 1.8 Å^{-1} and a small second peak at ~ 4.5 Å^{-1}, indicates that all three samples show a high degree of disorder. This is demonstrated further in Fig. 11 where scattering from the 'high titania' sample in thin film form (shallow angle geometry) is compared to scattering from the bulk (x-ray, transmission geometry[20]). Both data sets are at a similar stage of data reduction. Both curves are dominated by a first step peak primarily associated with Si–O first neighbor correlations, but the bulk sample also shows definite second and third peaks. For the thin film sample it is very difficult to determine any distinct higher-order correlations, although some evidence of residual structure in that region is visible. Due to the contamination by silicon Bragg reflections, and the large amount of statistical noise in the data produced by scattering from very small effective sample volumes, the information available from a Fourier transformation into real space is limited. Figure 12 shows the Fourier transform of the interference function (i.e., the pseudostructure factor) for the 'high titania' sample as an example of the r-space information obtainable.

The strong correlation visible at ~ 1.5 Å is associated with the Si–O distance. In bulk silica the Si–O first neighbor distance is 1.61 Å. However, the silicon-oxygen distance is reduced to 1.50 Å when taken out of the confines of the silica network, for example when part of an $Si(OH)_4$ unit. This may be further evidence that the silica network has become more disordered when in a thin film, and contrary to the case for the bulk material, there are few long silicon-oxygen chains and more hydrogen atoms terminating the network. There is little order apparent in the "$G(r)$" after the first main peak. In particular, interatomic distances resulting from O–Si–O (2.6 Å) and Si–O–Si (3.0 Å) bonds which

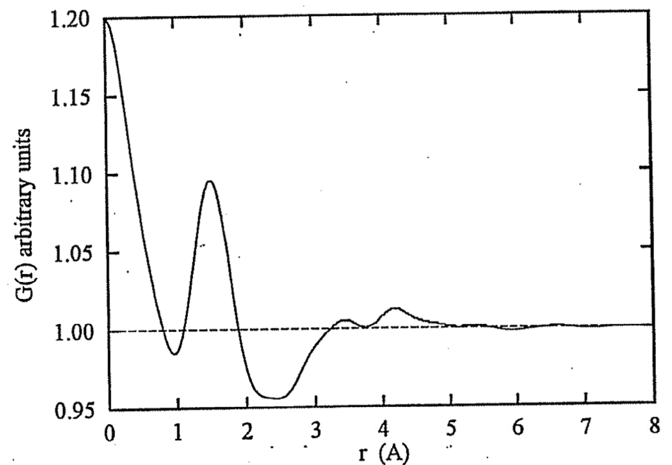

FIG. 12. Approximate pair distribution function for the "high titania" mixed sol-gel glass.

are prominent in $G(r)$ data from the bulk silica : titania sol-gels are not visible here.

D. Alumina and "glassy" carbon coatings

New data are presented here for Al_2O_3 films on silicon and for near-surface impregnated and heat-treated graphite. Table V shows the calculated characteristic penetration depths into the alumina coatings as a

TABLE V. Characteristic penetration depths for x-rays of various wavelengths and angles of incidence with respect to the alumina coatings.

α_i	α_i	Characteristic penetration depth t (Å)		
(°)	(rad)	$\lambda = 0.7$ Å	$\lambda = 1.04$ Å	$\lambda = 1.5$ Å
0.05	0.000873	78.9 (#91)	71.6 (#91, #96)	69.2 (#91, #96)
0.20	0.003491	9.9 μm	3.1 μm (#91, #96)	339.8 (#91)

function of wavelength and angle of incidence; the use of a synchrotron source enabled this two-variable investigation and hence allowed an additional check on the method. Although the use of longer wavelengths does limit the dynamic range of the data, it proved valuable for the study of these exceptionally thin, low atomic number films. It must be reiterated that t is defined to be the depth at which the incident radiation has fallen to $1/e$ of its original intensity. Some of the intensity therefore penetrates farther into the sample before it is absorbed/scattered. At an incident angle of 0.05°, at all wavelengths used, the bulk of the x-rays penetrates only the very top of the thin film, to characteristic depths up to ~70 Å. At $\alpha_i = 0.2°$ and the longest wavelength most of the film is examined, at shorter wavelengths penetration is through the ~5000 Å film into the substrate. The coating deposited with additional ion beam bombardment, labeled #91 in Table V and subsequent figures, was probed using all three x-ray wavelengths and at both angles of incidence used whereas the coating deposited by electron beam methods alone, labeled #96, was studied using only the longer wavelengths. Unfortunately, due to the very small sample volume probed at the lowest angles and longest wavelengths, the background contribution to the scattering pattern collected was relatively large and accurate isolation of the scattering of the coating was not possible. Figure 13, however, shows the data gathered at $\lambda = 1.04$ Å and at $\alpha_i = 0.2°$. This quite clearly shows that there is, in fact, *more* ordering in the ion beam bombarded sample, although the peaks are still relatively broad and it is probable that the crystallites are small. The two strong peaks at ~3.2 Å^{-1} and 4.4 Å^{-1} are attributable to the two strongest Al_2O_3 reflections (see Table VI). Spectra taken from coating #91 at $\lambda = 0.7$ Å and at $\alpha_i = 0.05°$ further strengthen the conclusion that this is indeed an ordered coating since the improved data quality (see Fig. 14) reveals additional Bragg-like peaks which are also attributable to the corundum form of alumina. It is important to keep in mind the fact that the data here represent an average over the whole volume probed, unlike TEM and related selected-area approaches, so crystallites included in an amorphous matrix will easily be observed (this does not, however, explain the apparent absence of Bragg-like features in the conventionally deposited sample, which would generally have been assumed to be polycrystalline. However, it surely provides evidence for the effectiveness of the shallow angle method.

TABLE VI. Crystalline d-spacings for the principal Bragg peaks arising from the corundum form of alumina; also shown is the associated Q-value in the context of the present work.

d (Å)	{h k l}	Q (Å^{-1})
4.12	1 0 0	1.53
3.48	0 1 2	1.81
2.55	1 0 4	2.46
2.38	1 1 0	2.64
2.17	0 0 6	2.90
2.09	1 1 3	3.01
1.96	2 0 2	3.20
1.74	0 2 4	3.61
1.60	1 1 6	3.93
1.56	210/211	4.04
1.52	122/018	4.15
1.41	2 1 4	4.47
1.34	302/125	4.68
1.28	2 0 8	4.92
1.23	1 1 9	5.09
1.19	2 2 0	5.28
1.16	3 0 6	5.42
1.15	2 2 3	5.48
1.10	0 2 10	5.72
1.08	1 3 4	5.83
1.05	3 1 5	6.01

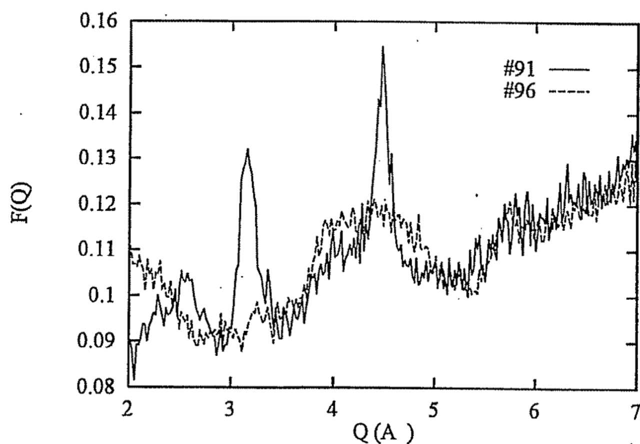

FIG. 13. Interference functions measured for the electron beam deposited Al_2O_3 coatings at $\lambda = 1.04$ Å and $\alpha_i = 0.2°$ (#91 was deposited with additional ion beam bombardment).

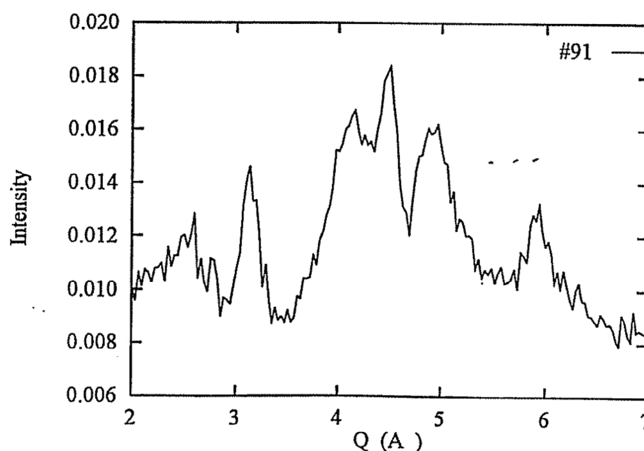

FIG. 14. Interference function for alumina coating #91 measured using $\lambda = 0.7$ Å and $\alpha_i = 0.05°$.

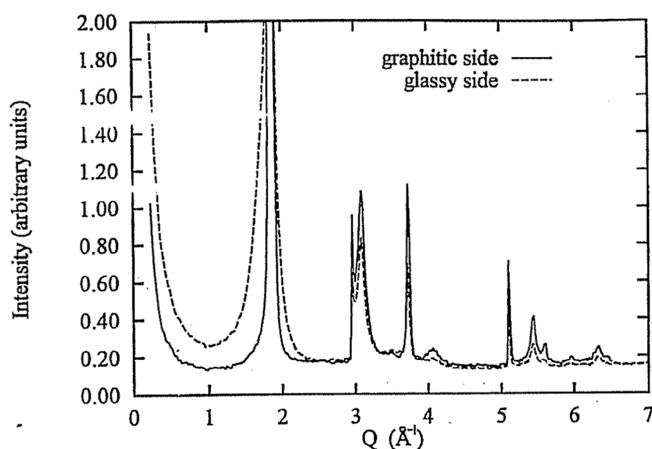

FIG. 15. Interference functions collected at $\lambda = 1.04$ Å and at $\alpha_i = 0.05°$ from the treated and the untreated faces of the graphite plate.

The diffraction spectra collected at $\lambda = 1.04$ Å and at $\alpha_i = 0.05°$ from the treated and the untreated faces of the graphite plate are shown in Fig. 15. It is immediately apparent that the impregnation and heat-treated face has indeed been altered at the level of atomic structure, but that it is not truly amorphous (or glass-like) but rather appears to be a disordered graphitic network. Given the attributes of the treated surface, the most likely explanation for the significant broadening of the graphite Bragg peaks is that the treatment induces greater interlayer binding and distorts the original planar geometry.

VII. CONCLUSIONS

It will be apparent from the summary given above, and the publications list, that the method has been shown to be able to generate results of interest to both the academic and the industrial materials scientist. However, there are important limitations that pertain to the method, at least in its present state of development and for application to amorphous films and coatings.

(1) The substrate (and the film) must be flat on the scale of the angle of incidence, be smooth on the scale of the penetration depth of the x-rays, and have no macroscopic pinholes or other discontinuities. This effectively eliminates a great many "real" materials science samples. The problem is made worse by the need for these conditions to be satisfied over large areas if the experimental statistics are to be adequate (remember, these are diffuse, not Bragg scatterers).

(2) When trying to eliminate the (crystalline, Bragg scattering) contribution of the substrate from the diffuse spectrum scattered from an amorphous film, it is necessary to operate at wavelengths and/or angles of incidence such that the characteristic penetration depth for the x-rays is small compared to the physical thickness of the film. This limits the applicability of the method, especially for light-atom systems and for those films/coatings which cannot be deposited thicker.

(3) The effective minimum angles of incidence are determined by the need to gather adequate statistics, and such instrument characteristics as the acceptance angle of the slit package which acted as the detector collimation. Even with the longest slit package available for this work the acceptance angle was 0.07°, which meant that, irrespective of any additional limitations imposed by (1), the minimum angle of incidence was $\sim 0.05°$. This limitation is coupled with the need to use as short a wavelength as is practicable in order to get as high a $Q_{\max}$ as possible (which is important for amorphous materials in the context of the real-space resolution required). These limitations meant that it was very difficult to get information from systems of low atomic number (below Si, O or thereabouts, but obviously depending on the nature of other scatterers present in the sample).

(4) The lowest detector angle is limited by simple geometric/instrumental constraints, associated with the choice of the angle of incidence and the level of "background" scattering that arise from it, to about 3–4°, which necessarily reduces the extent of the scattering data at the low-Q end of the spectrum. In practice data were often not usable for this reason, and because of the associated high background at low angles, until after a Q value of ~ 1 Å.

(5) The above problems are associated with others arising from any attempt to extract quantitative information from the spectra measured (i.e., to measure a structure factor on an absolute scale and hence be able to extract from that a quantitative pair correlation function by Fourier transformation):

The background scatter is impossible to measure in any way that is of real use since there is no such thing as a "null" plate that one could use in place of the sample. This contribution therefore has to be subtracted in an approximate fashion, with the result that errors, particularly at low Q, could be significant. However, there is no reason to think that this scattering profile will be anything other than smooth, so in itself it poses no serious difficulty.

Basic data reduction for both conventional and shallow angle x-ray diffraction can be carried out in a similar manner: corrections are made for detector dead time, changes in incident beam current, and beam polarization effects. A further correction is needed in the shallow angle geometry to account for the fact that the x-ray beam collected at the detector is actually scattered from the *refracted* beam in the sample; this produces a small shift in the measured scattering angle 2θ. However, corrections to the data which rely on a knowledge of the optical path length associated with the detected x-rays (absorption, multiple scattering) cannot be carried out

in practice. Given the fact that the x-rays have a range of possible penetration depths, the straightforward analytical solutions to this problem (which we did generate and attempt to use) no longer pertain. It may be possible, given the time, to correct the data in an indirect fashion using a Monte Carlo simulation approach, but this does not seem to be a particularly cost-effective exercise.

Combining these problems, with the general difficulty associated with a lack of knowledge of the actual density of the films in their as-deposited state, one is left with only a pragmatic solution based on fitting a set of Chebyshev polynomials through the data and thereby isolating an approximation to the structure factor. This provides data in which the peak positions are reasonably well defined, but the peak amplitudes are not.

The overall conclusion is therefore that the method has been shown to have limitations in the study of amorphous systems as a whole since it is not fully quantitative, but is entirely adequate, even useful, in the context of well-defined materials science problems associated with suitable samples where differences between samples, or some other relative effect, is at the root of the solution.

ACKNOWLEDGMENTS

We are grateful to the following for supplying samples and for their permission to publish the data: I. C. Bassignala (Northern Telecom Technologies Ltd., Canada) for alumina coatings; S. Fraser (Megatech Ltd., U.K.) and T. S. Ozycz (Graphite Die Mold Inc., USA) for the treated (glassy) graphite; W. Paul and P. Wickboldt (Harvard University) for a–Si : Ge : H films; M. E. Smith and P. J. Dirken (University of Kent at Canterbury) for silica : titania spun films; J. I. B. Wilson, M. G. Jubber, N. A. Morrison, I. C. Drummond, and P. John (Heriot-Watt University, U. K.) for CVD diamond coatings on silicon and on steel, for free diamond films, and for a–Si : C : H films on silicon wafers. We acknowledge the financial support of the SERC (now EPSRC) and the use of the SRS at Daresbury for the diffraction measurements, and the University of Kent at Canterbury.

REFERENCES

1. W. P. G. Lim and C. Ortiz, J. Mater. Res. **2**, 471 (1987).
2. T. M. Burke, D. W. Huxley, R. J. Newport, and R. Cernik, Rev. Sci. Instrum. **63**, 1150 (1992).
3. T. M. Burke, *An x-ray and neutron diffraction study of amorphous hydrogenated carbon,* Ph.D. Thesis, University of Kent at Canterbury, U.K. (1994).
4. (a) *Synthetic Diamond: Emerging CVD Science and Technology,* edited by K. E. Spear and J. D. Dismukes (Wiley & Sons, Chichester, U.K., 1994); and (b) A. H. Lettington, in *Diamond and Diamond-like Films and Coatings,* edited by J. C. Angus, R. E. Clausing, L. L. Horton, and P. Koidl (Plenum Publishing, New York, 1991).
5. J. S. Rigden, T. M. Burke, R. J. Newport, J. I. B. Wilson, M. G. Jubber, N. A. Morrison, and P. John, J. Electrochem. Soc. **143,** 1033 (1996); and J. S. Rigden and R. J. Newport, in *Diamond Materials IV,* edited by K. Ravi and J. Dismukes (Electrochem. Soc. Inc., NJ, 1995), p. 473.
6. M. G. Jubber, J. I. B. Wilson, I. C. Drummond, P. John, and D. K. Milne, Vacuum **45**, 499 (1994).
7. N. A. Morrison, I. C. Drummond, C. Garth, P. John, D. K. Milne, G. P. Smith, M. G. Jubber, and J. I. B. Wilson, Proc. *Diamond Films '95,* Barcelona, 1995, and Diamond and Related Mater. (in press); also, U.K. patent application 9211107.9, 1992.
8. J. Franks, J. Vac. Sci. Technol. **A7**, 2307 (1989).
9. J. K. Walters and R. J. Newport, J. Phys.: Condens. Matter **7**, 1755 (1995).
10. F. Ibrahim, J. I. B. Wilson, and P. John, J. Non-Cryst. Solids **164–166**, 1051 (1993); and A. Cook, A. G. Fitzgerald, F. Ibrahim, J. I. B. Wilson, and P. John, Mikrochem. Acta **114/115**, 255 (1994); and F. Ibrahim, J. I. B. Wilson, P. John, A. G. Fitzgerald, and A. Cook. J. Non-Cryst. Solids **175,** 195 (1994); and F. Ibrahim, J. I. B. Wilson, and P. John, J. Non-Cryst. Solids **191,** 191 (1995).
11. T. M. Burke, P. J. R. Honeybone, D. W. Huxley, R. J. Newport, Th. Frauenheim, P. Blaudeck, Th. Kohler, and C. Hotham, in *Novel Forms of Carbon,* edited by C. L. Renschler, J. J. Pouch, and D. M. Cox (Mater. Res. Soc. Symp. Proc. **270**, Pittsburgh, PA, 1992), p. 97; P. J. R. Honeybone, J. K. Walters, D. W. Huxley, R. J. Newport, W. S. Howells, J. Tomkinson, and C. Hotham, J. Non-Cryst. Solids **169**, 54 (1994).
12. W. Paul, J. H. Chen, E. Z. Liu, A. E. Wetsel, and P. Wickbolt, J. Non-Cryst. Solids **164–166**, 1 (1993).
13. C. J. Brinker and G. W. Scherer, *Sol-Gel Science: The Physics and Chemistry of Sol-Gel Processing* (Academic Press, Inc., San Diego, CA, 1990).
14. M. Itoh, H. Hattori, and K. J. Tanabe, Catal. **35**, 225 (1974).
15. M. E. Smith and H. J. Whitfield, J. Chem. Soc., Chem. Commun. **6**, 723 (1994).
16. P. J. Dirken, M. E. Smith, and H. J. Whitfield, J. Phys. Chem. **99**, 395 (1995).
17. T. J. Bastow, A. F. Moodie, M. E. Smith, and H. J. Whitfield, J. Mater. Chem. **3**, 697 (1993).
18. J-J. Cheng and D-W. Wang, J. Non-Cryst. Solids **100**, 288 (1988).
19. M. Emili, L. Incoccia, S. Mobilio, G. Fagherazzi, and M. Guglielmi, J. Non-Cryst. Solids **74**, 129 (1985).
20. J. S. Rigden, R. J. Newport, M. E. Smith, P. J. Dirken, and G. Bushnell-Wye, J. Mater. Chem. **6**, 337 (1996).
21. P. J. Dirken, R. Dupree, and M. E. Smith, J. Mater. Chem. **5**, 1261 (1995).
22. D. E. Bornside, C. W. Macosko, and L. E. Scriven, J. Imag. Technol. **13**, 122 (1987).
23. G. H. Vineyard, Phys. Rev. B **26**, 4146 (1982).
24. G. Bushnell-Wye and R. Cernik, Rev. Sci. Instrum. **63**, 999 (1992).
25. B. E. Warren, *X-ray Diffraction* (Dover Publications Inc., New York, 1990).
26. P. John, C. Graham, D. K. Milne, M. G. Jubber, and J. I. B. Wilson, Proc. *Diamond Films '95,* Barcelona, 1995, and Diamond and Related Mater. (in press).
27. S. R. Elliot, Adv. Phys. **38**, 1 (1989).